

Photon-counting digital holography

Nazif Demoli*^{a,c}, Hrvoje Skenderović^{a,c}, Mario Stipčević^{b,c}, Mladen Pavičić^c

^aInstitute of Physics, Bijenička cesta 46, HR-10000 Zagreb, Croatia; ^b(RBI) Ruđer Bošković Institute, Bijenička cesta 54, HR-10000 Zagreb, Croatia; ^cCEMS, Photonics and Quantum Optics Unit, RBI

ABSTRACT

Digital holography uses electronic sensors for hologram recording and numerical method for hologram reconstruction enabling thus the development of advanced holography applications. However, in some cases, the useful information is concealed in a very wide dynamic range of illumination intensities and successful recording requires an appropriate dynamic range of the sensor. An effective solution to this problem is the use of a photon-counting detector. Such detectors possess counting rates of the order of tens to hundreds of millions counts per second, but conditions of recording holograms have to be investigated in greater detail. Here, we summarize our main findings on this problem. First, conditions for optimum recording of digital holograms for detecting a signal significantly below detector's noise are analyzed in terms of the most important holographic measures. Second, for time-averaged digital holograms, optimum recordings were investigated for exposures shorter than the vibration cycle. In both cases, these conditions are studied by simulations and experiments.

Keywords: Holography, digital holography, holographic interferometry, photon counting, fringe analysis

1. INTRODUCTION

Digital holography employs the charge-coupled device (CCD or CMOS) sensors for recording holographic patterns then followed by numerical reconstruction.¹ That enabled the development of advanced holography applications, such as visualization of living cells,^{2,3} flow analysis^{4,5} high-speed volumetric imaging,⁶ or dynamic measurements in real-time.⁷ However, in some cases, the useful information is concealed in a very wide dynamic range of illumination intensities and successful recording requires an appropriate dynamic range of the sensor. For a CCD sensor, the dynamic range can be estimated by the ratio of the maximum achievable nonsaturating signal (full-well capacity) and the sensor noise and by the digitalization of the output of the sensor. Mostly, the CCD or CMOS sensors have 8 bit or 10 bit, and rarely up to 16 bit depth, which is sufficient for most holographic applications. Generally, a problem arises in detecting a signal that is of much lower power than the sensor noise. Then, depending on the reference beam intensity, the fringe pattern is either obscured by noise (for equal beam intensities) or, otherwise, flattened by the digitalization process. A possible approach to this problem is to use a photon-counting detector (PCD).⁸⁻¹⁰ Such detectors possess counting rates of the order of tens to hundreds of millions counts per second (cps), allowing sensitivity at the fundamental quantum limit and fast data acquisition. We have investigated the optimum recording conditions for detecting a weak signal significantly below PCD noise in terms of the most important holographic measures, namely, the fringe visibility (V) (or contrast) and signal-to-noise ratio (SNR), and in relation to the main recording parameters. First, expressions for the V and SNR are evaluated for digital holograms (DHs) and then, it is shown that the optimum recording DH parameters are possible to estimate theoretically and to implement experimentally.

For time-averaged digital holograms (TADHs), this problem becomes even more complex due to the generally imposed condition of having the hologram exposures either equal or long compared to the vibration period.¹¹ This condition is difficult to satisfy in cases with very low frequency vibrations or with the presence of some environmental instabilities. To overcome these problems and find more general approach, we have investigating the possibility of recording many short exposures instead of long ones. For recording TADHs, instead of one PCD we used an array of PCDs assembled as a compact camera (SPC2).

*demoli@ifs.hr; phone 385 1 4698882; fax 385 1 4698889; demoli.ifs.hr

2. THEORY

2.1 Digital hologram parameters

Exposure of a sensor is described as $E(x, \tau) = \int_0^\tau I(x, t) dt$, where τ is the exposure time and $I(x, t)$ is the intensity of the interference of two beams, the signal (or object) $I_s(x)$ and reference $I_r(x)$, and where (x) denotes the spatial coordinate (one-dimensional for simplicity). The intensity $I(x, t)$ describes a fringe pattern

$$I(x, t) = I'_0(x) + 2\sqrt{K(x)}I_s(x)\cos[\varphi'(x, t)], \quad (1)$$

where $I'_0(x) = I_0(x) + I_n(x)$ is the background intensity described as a sum of its deterministic part, $I_0(x) = I_r(x) + I_s(x)$, and the additive noise, $I_n(x)$; $K(x)$ denotes the beam ratio, $K(x) = I_r(x)/I_s(x)$; and the phase $\varphi'(x, t) = \varphi(x) + \varphi_n(x, t)$ is also a sum of a deterministic part, $\varphi(x)$, and the phase noise $\varphi_n(x, t)$. The phase noise, originating from instabilities during holographic exposure, accumulates over time.¹² Thus, the exposure is

$$E(x, \tau) = I_s(x)[1 + K(x) + K_n(x)]\tau + 2I_s(x)\sqrt{K(x)}\tau \cos[\varphi(x)] \psi_n(x, \tau), \quad (2)$$

where the expression for the phase noise $\psi_n(x, \tau)$ is given by $\psi_n(x, \tau) = 1 - \tan[\varphi(x)](1/\tau) \int_0^\tau \varphi_n(x, t) dt - (1/2\tau) \int_0^\tau \varphi_n^2(x, t) dt + \dots$, and was derived by expanding the cosine function $\cos[\varphi(x) + \varphi_n(x, t)]$ into Taylor series around $\varphi(x)$, $\varphi_n(x, t) < \varphi(x)$, and expressing only the first few terms of the series. $K_n(x)$ is ratio of the intensities (or photon counts) of the PCD noise and the signal beam, $K_n(x) = I_n(x)/I_s(x)$. The expressions for two most important holographic measures, namely the fringe visibility (V) and signal-to-noise ratio (SNR) can be derived from Eq. (2),

$$V = \frac{2\sqrt{K}}{1+K+K_n} \psi_n(\tau), \quad (3)$$

$$SNR = 2 I_s \frac{\sqrt{K} \tau}{\sigma(\tau)} \psi_n(\tau). \quad (4)$$

The experimentally recorded fringe patterns were analyzed by fitting the measured data to a function: $E_{FIT}(x) = A + B \cdot \cos(Cx + D)$, where C is determined from the experimental setup, $C = 2\pi \sin \alpha / \lambda$, α is angle between the beams, and λ is the wavelength. The A and B are of the form: $A = I_s[1 + K + K_n]\tau$ and $B = 2I_s(K)^{1/2} \tau \psi_n(\tau)$, as evident by comparing $E_{FIT}(x)$ and Eq. (2). The standard deviation can be defined here as $\sigma(\tau) = \langle [E(x, \tau) - E_{FIT}(x)]^2 \rangle^{1/2}$.

2.2 Time-averaged digital holograms

The reconstructed TADHs can be described by means of

$$M(x) = \frac{1}{\tau} \int_0^\tau \exp[i\Phi(x)\sin 2\pi f t] dt, \quad (5)$$

where f is the vibration frequency and $\Phi(x) = 2\pi h(x)/\lambda$, where $h(x)$ is the vibration amplitude. $M(x)$ cannot be solved analytically for arbitrary τ values, but can be expressed by the following series:

$$M(x) = J_0(x) + \frac{4}{\omega\tau} \sum_{k=1}^{\infty} \left[\frac{1}{2k} J_{2k}(x) \cos k\omega\tau \sin k\omega\tau + \frac{i}{2k-1} J_{2k-1}(x) \sin(2k-1)\omega\frac{\tau}{2} \sin(2k-1)\omega\frac{\tau}{2} \right], \quad (6)$$

where J are Bessel functions and $\omega = 2\pi f$. According to Eq. (6), the higher terms modify the Bessel function of the first kind, $J_0(x)$, when the exposure time τ is smaller than the period $T = 1/f$ as shown in Fig. 1. However, these conditions can be also fulfilled by averaging many TADHs with randomized short exposures ($\tau \ll T$), where we define the average fringe function (AFF),¹⁰ $AFF = (1/L) \sum_{i=1}^L |M(x)|$, and where L is the number of recorded holograms.

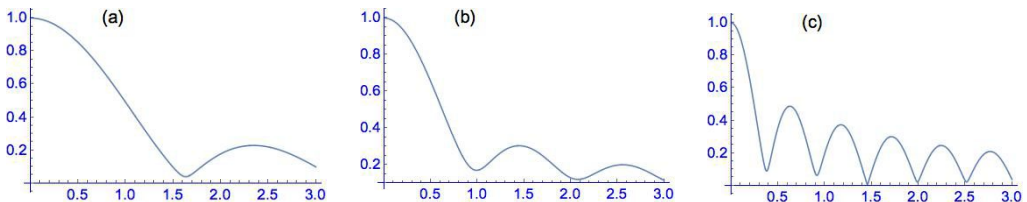


Figure 1. The characteristic fringe function ($|M(x)|$) for (a) $\tau = T/8$, (b) $\tau = T/4$, (c) $\tau = T$.

3. EXPERIMENTAL DEVICE

We have configured two types of optical setups, one of a Mach-Zehnder type (employing PCD for detecting a weak signal: 0.44 cps, significantly below noise: 21 cps) and the other of a lensless Fourier (or quasi-Fourier) type (employing SPC2 for recording TADHs). In both setups we have used a He-Ne laser (wavelength $\lambda = 632.8$ nm) as light source, coupled in free space into a single-mode optical fiber, and a motorized XY stage for motion control of detectors (shown in Fig. 2). Photon detections are counted by a digital counter (SR400). A home-made software was used to control the scanning of the XY translation stage as well as the data acquisition process. Experimental details of both setups are given elsewhere.^{9,10}

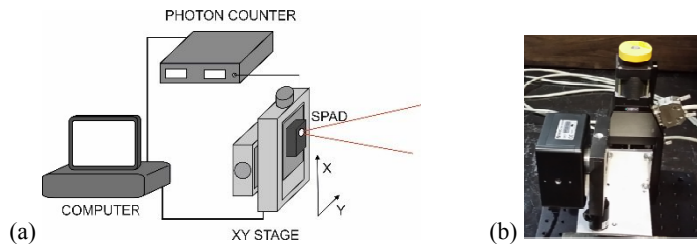


Figure 2. Motion control of the motorized XY stage with detector presented as (a) scheme and (b) photo.

3.1 Photon-counting detector

The PCD is based on a single-photon avalanche photodiode (SPAD) (model SAP500, LC) selected for low noise, cooled and operated in Geiger mode. The detector (shown in Fig. 3) features maximum count rate of 10 Mcps, dark count rate of 21 cps, dead time of 23 ns and detection efficiency about 60% at 632 nm. A pinhole of diameter $10 \mu\text{m}$ is mounted in front of the SPAD which was moved in $10 \mu\text{m}$ steps to form a matrix of 512×512 synthetic 'pixels'.



Figure 3. Photon-counting detector used for recording digital holograms with low light levels.

3.2 Single-photon camera

The SPC2 features round pixels with sensitive area of $20 \mu\text{m}$ in diameter, arranged in a square array of 32×32 pixels with a pitch of $100 \mu\text{m}$. The footprint of the each pixel cell is shown in Fig 4(a). Visible are the circular active area of the SPAD, guard ring around it, the area accommodating amplification and quenching circuit (VLQC), gate switch and 8 master-slave flip-flops that form an 8-bit counter with a latch memory. Since this results in the filling factor of only $\sim 3\%$, which is not suitable for taking holograms, the whole camera was mounted on and XY stage and moved around such that the sensitive area would completely fill the desired data collection area. To this end, the camera was first moved along x direction in 10 steps of $10 \mu\text{m}$ and then moved in y direction by one step of $10 \mu\text{m}$ and so forth until 10×10 pixel array is swept, as shown in Fig. 4(b). Thus, the TADHs are obtained with total of 320×320 pixels of size $10 \times 10 \mu\text{m}$. Larger pictures were obtained by concatenating 2×2 (640×640 pixels) or 3×3 (960×960 pixels) of these blocks.



Figure 4. (a) Footprint of a single pixel cell in SPC2 (reprinted from [13] with the permission from MPD), (b) schematic diagram of camera walk in x - y plane.

4. RESULTS

4.1 The fringe visibility curves

Equation (3) was used to calculate the contrast curves for wide range of the K and K_n parameters. Assuming $\psi_n(\tau) = 1$ the curves are shown in Fig. 5. From Fig. 5 (a) we see that the larger K_n provides the lower maximum for V that is also shifted to higher K values, i.e. $K_{max} = 1 + K_n$. From Fig. 5 (b) we see that higher K values yield lower (but more robust against the noise) V values.

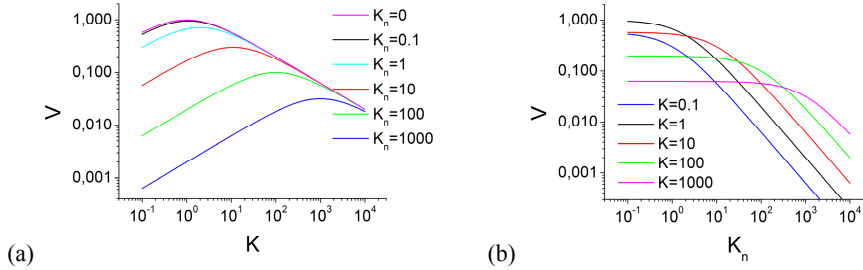


Figure 5. The fringe visibility as a function of K and K_n (numerical simulations).

4.2 Determination of V and SNR measures from experimental measurements

The sinusoidal gratings were recorded for a wide range of the K values and fixed K_n parameter for our PCD. The following protocol was applied: (i) set the K value, (ii) record holographic grating along the same horizontal line repeatedly, and (iii) calculate the amplitude parameters A and B , standard deviation $\sigma(\tau)$, and measures V and SNR . Table 1 shows these measures. As predicted theoretically, see Eq. (3), the visibility is nearly constant within the selected K value, while the obvious differences in quality of the grating are revealed clearly by the SNR measure.

Table 1. The measures V and SNR calculated from experimental values.

K	1				4				10				100				1000			
τ (s)	0.1	1	10	100	0.1	1	10	100	0.1	1	10	100	0.1	1	10	100	0.1	1	10	100
V	0.03	0.05	0.04	0.04	0.06	0.08	0.08	0.08	0.12	0.12	0.12	0.11	0.20	0.21	0.21	0.14	0.16	0.16	0.15	0.08
SNR	1.1	6.4	19.6	43.7	8.2	10.9	35.4	50.8	5.5	19.6	37.5	42.3	12.1	18.9	20.4	17.1	11.3	11.4	10.7	10.0

4.3 Accurate determination of the experimental K_n ratio

The actual K_n value is the ratio of the noise and signal intensity values detected by the PCD. Since direct K_n measurement is not accurate (signal intensity is much smaller than the detector's noise), we performed the following steps: first, we calculated V values as a mean of individual values obtained for each τ , and then, we performed a least-squares fit of data points to the theoretical curve in Eq. (3) with K_n as a single free parameter and $\psi_n(\tau) = 1$. This procedure yielded the value $K_n = (48.0 \pm 8.5)$, derived from the maximum of the fitted curve from Fig. 6.

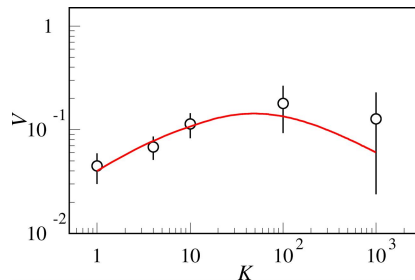


Figure 6. The fringe visibility as a function of K . Values calculated from experimental measurements are denoted by circles and the least-squares fit is shown as the solid curve.

4.4 DH reconstructions of a weak signal

To record DHs, a detail, shown in Fig. 7(a) from the NBS 1963A resolution target, was positioned in the object arm of the Mach-Zehnder interferometer as a transparent object. The reference arm was adjusted to obtain the quasi-Fourier configuration. The recorded holograms (size: 512×512 pixels) are reconstructed by performing the Fourier transform operation. From Table 1 it is apparent that the best reconstructions (i.e. the highest SNR values achieved at longer exposures) can be expected for $K = 4$ and 10. This is indeed confirmed by the experimental DHs that we recorded for various values of K and τ . The DH reconstructions shown in Fig. 7(b-e) illustrate this concept.

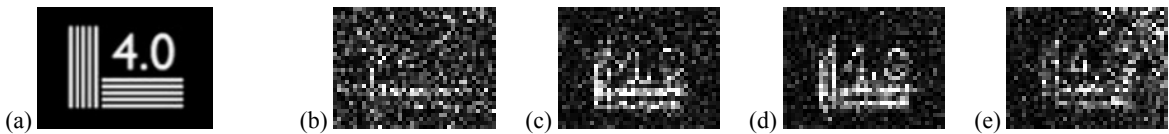


Figure 7. (a) Detail from the NBS 1963A resolution target. Reconstructed DHs for $\tau = 50$ ms: (b) $K = 1$, (c) $K = 4$, (d) $K = 10$, (e) $K = 100$.

4.5 TADH reconstructions for exposures smaller than the vibration period

The TADHs were recorded by employing SPC2 and a silicon wafer as an input object. In order to obtain good quality TADHs, we had to solve several problems. First, in each 320×320 picture, the tiles of 10×10 pixels belong to the same physical pixel which differs from other pixels in dark counts, afterpulsing probability and quantum efficiency. This created a "tiling" effect in the recorded hologram that resulted in a repetitive pattern of smudges after reconstruction. This was removed by a pixel calibration algorithm that we developed. As illustrated for vibration mode 1218 Hz (Fig. 3 in Ref. 10), a halo in the center was removed by the subtraction method.¹⁴ The echo is due to the inevitable progressive change of the laser beam phase between scanned lines in y direction. The period of 32 pixels refers to size of the same-phase array of physical pixels. This finding led us to another idea: we modified the steering program such that 10×10 pixels in the basic block were taken in random rather than in orderly manner. While this did not affect tiling and halo effects, it did completely remove the echo. In Fig. 8 it is demonstrated how the averaging of TADHs with exposure time $\tau \ll T$ clearly reveals the characteristic Bessel function fringes for the vibration mode of 220 Hz. Figure 9 comprises the numerical SNR (circles) and the SNR calculated from experimentally obtained data (crosses), the former were adapted to the experimental values and plotted on the same scatter chart. Apparently, an increasing SNR trend over the number of recorded holograms can be well matched in the middle part of the graph ($100 \leq L \leq 1000$). We presume that the observed mismatches noticed for other L values are due to the noise and saturation properties of the SPC2.

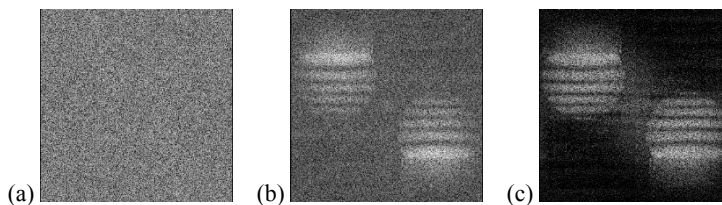


Figure 8. The reconstructed TADHs for $\tau = 1$ ms, (a) $L = 1$, (b) $L = 100$, and (c) $L = 2000$.

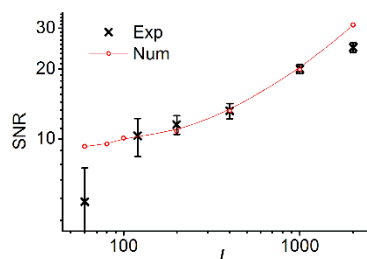


Figure 9. The SNR for both numerical and experimental values.

5. CONCLUSIONS

In this study, we have shown that applying the photon-counting approach, originally acquired holographic information can be efficiently preserved by employing the high dynamic range of the PCD. It is demonstrated that the optimum values of recording parameters can be evaluated theoretically and as well implemented experimentally. Consequently, a weak signal (0.44 cps, or the equivalent of 0.23 aW) hidden well below noise level (21 cps) has been successfully detected. It is also found that increasing the contrast of fringes does not necessarily improve the more important *SNR* measure and that, in cases of nearly constant contrast, the *SNR* clearly reveals differences in the quality of holographic recordings.

For vibrating surfaces, the conditions are found for satisfactory hologram recordings with exposure times much shorter than the vibration period. For this purpose, we have introduced the average fringe function and randomized short exposures. Thus, it is clearly demonstrated that the *SNR* increases by the number of averaged holograms and that the potential of the photon-counting time-averaged digital holography can be fully extended to arbitrary vibration frequencies suggesting that as well the reliable measurements are possible even in rather severe environmental conditions.

Acknowledgments

This study is supported by Croatian Science Foundation (project: IP-2014-09-7515). Authors are grateful to Micro Photon Devices for loan of the SPC2 camera.

REFERENCES

- [1] Osten, W., Faridian, A., Gao, P., Körner, K., Naik, D., Pedrini, G., Singh, A.K., Takeda, M. and Wilke, M., "Recent advances in digital holography [Invited]," *Appl. Opt.* 53(27), 44-63 (2014).
- [2] Carl, D., Kemper, B., Wernicke, G. and Von Bally, G., "Parameter-optimized digital holographic microscope for high-resolution living-cell analysis," *Appl. Opt.* 43(36), 6536-6544 (2004).
- [3] Memmolo, P., Miccio, L., Finizio, A., Nett, P.A. and Ferraro, P., "Holographic tracking of living cells by three-dimensional reconstructed complex wavefronts alignment," *Opt. Lett.* 39(9), 2759-2762 (2014).
- [4] Demoli, N., Vukicevic, D., and Torzynski, M., "Dynamic digital holographic interferometry with three wavelengths," *Opt. Express* 11(7), 767-774 (2003).
- [5] Yourassowsky, C. and Dubois, F., "High throughput holographic imaging-in-flow for the analysis of a wide plankton size range," *Opt. Express* 22(6), 6661-6673 (2014).
- [6] Saglimbeni, F., Bianchi, S., Lepore, A. and Di Leonardo, R., "Three-axis digital holographic microscopy for high speed volumetric imaging," *Opt. Express* 22(11), 13710-13718 (2014).
- [7] Demoli, N., "Real-time monitoring of vibration fringe patterns by optical reconstruction of digital holograms: mode beating detection," *Opt. Express* 14(6), 2117-2122 (2006).
- [8] Yamamoto, M., Yamamoto, H. and Hayasaki, Y., "Photon-counting digital holography under ultraweak illumination," *Opt. Lett.* 34(7), 1081-1083 (2009).
- [9] Demoli, N., Skenderović, H. and Stipčević, M., "Digital holography at light levels below noise using a photon-counting approach," *Opt. Lett.* 39(17), 5010-5013 (2014).
- [10] Demoli, N., Skenderović, H. and Stipčević, M., "Time-averaged photon-counting digital holography," *Opt. Lett.* 40(18), 4245-4248 (2015).
- [11] Brown, G.M., Grant, R.M. and Stroke, G.W., "Theory of holographic interferometry," *J. Acoust. Soc. Am.* 45(5), 1166-1179 (1969).
- [12] Demoli, N., "Use of optical fiber bundle in digital image plane holography," *Opt. Quant. Electron.* 45(8), 861-871 (2013).
- [13] Bellisai, S., Ferretti, L., Villa, A., Ruggeri, A., Tisa, S., Tosi, A. and Zappa, F., "Low-power 20-meter 3D ranging SPAD camera based on continuous-wave indirect time-of-flight," *Proc. SPIE* 8375, 83750E-83750E-7 (2012).
- [14] Demoli, N., Meštrović, J. and Sović, I., "Subtraction digital holography," *Appl. Opt.* 42(5), 798-804 (2003).